
AFRL-OSR-VA-TR-2014-0303

# STANFORD CENTER FOR MILITARY PHOTOMEDICINE

Christopher Contag
LELAND STANFORD JUNIOR UNIV CA

09/08/2014
Final Report



Air Force Research Laboratory
AF Office Of Scientific Research (AFOSR)/ RTB
Arlington, Virginia 22203
Air Force Materiel Command

# REPORT DOCUMENTATION PAGE

*Form Approved*
*OMB No. 0704-0188*



| **1. REPORT DATE** *(DD-MM-YYYY)* | **2. REPORT TYPE** | **3. DATES COVERED** *(From - To)* |
|---|---|---|
| 8/17/2014 | Final Performance Report | 01-Sep-2010 to 31-Dec-2013 |

**4. TITLE AND SUBTITLE**

Stanford Center for Military Photomedicine

**5a. CONTRACT NUMBER**

FA9550-10-1-0503

**5b. GRANT NUMBER**

**5c. PROGRAM ELEMENT NUMBER**

**6. AUTHOR(S)**

Christopher H. Contag, Daniel Palanker and Mark Schnitzer

**5d. PROJECT NUMBER**

**5e. TASK NUMBER**

**5f. WORK UNIT NUMBER**

**7. PERFORMING ORGANIZATION NAME(S) AND ADDRESS(ES)**

Stanford University
450 Serra Mall
Stanford, CA 94305-2004

**8. PERFORMING ORGANIZATION REPORT NUMBER**

**9. SPONSORING / MONITORING AGENCY NAME(S) AND ADDRESS(ES)**

AFOSR/NE, MFEL Program
Attn: Dr. Howard Schlossberg
875 North Randolph Street, Room 3112, Suite #325
Arlington, VA 22203

**10. SPONSOR/MONITOR'S ACRONYM(S)**

**11. SPONSOR/MONITOR'S REPORT NUMBER(S)**

**12. DISTRIBUTION / AVAILABILITY STATEMENT**

Public information

**13. SUPPLEMENTARY NOTES**

**14. ABSTRACT**

This project was aimed at developing clinically-deployable instrumentation for restoration of sight and hearing, and rapid, high-resolution in vivo imaging. Restoration of sight was accomplished using photovoltaic sub-retinal prosthesis in which photovoltaic arrays (70 um pixel size) restored visual acuity in rats with retinal degeneration to half of normally-sighted controls. In the field of retinal plasticity following ocular injury, we demonstrated closure of the retinal damage zone (under 200 um) and migration/rewiring of photoreceptors. For high-resolution imaging we have miniaturized confocal microscopes to fit into hand-held devices, with wide-field guidance, and have optimized the software to represent data as H&E stained sections—this point-of-care tool can rapidly assess tissue viability for guided debridement. We have also developed a clinically deployable second-harmonic generation microendoscope that reveals specific patterns of tissue and cellular micro-architecture, and visualized sarcomere lengths and twitch contraction dynamics, and abnormalities in individual striated muscle fibers of humans. This tool was further modified for neurotology to visualize the inner ear and guide placement of cochlear implants after blast injury.

**15. SUBJECT TERMS**

restoration of sight, restoration of hearing, miniature microscopes, retinal implants. advanced surgical tools,

| **16. SECURITY CLASSIFICATION OF:** | | | **17. LIMITATION OF ABSTRACT** | **18. NUMBER OF PAGES** | **19a. NAME OF RESPONSIBLE PERSON** |
|---|---|---|---|---|---|
| **a. REPORT** | **b. ABSTRACT** | **c. THIS PAGE** | | | **19b. TELEPHONE NUMBER** *(include area code)* |

# AFOSR Final Performance Report

Project Title: Stanford Center for Military Photomedicine

Award Number: FA9550-10-1-0503

Program Manager: WILLIAM P. ROACH, Ph.D.
AFOSR/RTB
875 North Randolph Road
Suite 325, Room 3112
Arlington, VA 22203-1768

Principle Investigator: Prof. Christopher Contag
Stanford University, Department of Pediatrics - Neonatology
Email: ccontag@stanford.edu
Phone: 650-725-6583

Co-Investigators: Prof. Daniel Palanker
Stanford University, Department of Ophthalmology & HEPL
Email: palanker@stanford.edu
Phone: 650-725-0059

Co-Investigators: Prof. Mark Schnizter
Stanford University, Department of Biology and of Applied Physics
Email: mschnitz@stanford.edu
Phone: 650-498-9388

**FINAL REPORT: STANFORD CENTER FOR MILITARY PHOTOMEDICINE**

Principal Investigator: Professor Christopher Contag
Co-Investigator: Professor Daniel Palanker

Reporting Period: 1 September 2010 – 31 December 2013

## A. OVERVIEW:

The Stanford Center for Military Photomedicine, through its support from the Air Force Office of Scientific Research (AFOSR), developed an interdisciplinary and collaborative program to advance military medicine in several areas of critical importance. The Stanford Military Photomedicine program has taken a multifaceted approach to understanding the molecular and cellular basis of tissue damage and developing sophisticated means of tissue repair and restoration of function. The team consisted of biologists, engineers, physicists, and chemists working together to address these of investigation with a diversity of disciplines. The research was based on a solid foundation in each of the areas of investigation and sought thoughtful innovation that would push the limits of tool development.

There were four thematic research areas in this center: (**1**) Restoration of hearing loss and in-vivo advanced microscopy. (**2**) The mechanism of damage and repair of wounds. Assessing the extent of tissue damage in vivo required the development of new tools and therefore this thematic area was also linked to the fourth thematic area of advanced microscopy. (**3**) The third thematic area was sight, and there were three projects in this area (a) Development of surgical techniques for transparent ocular tissues. (b) Development of the animal models of traumatic retinal injury and studies of associated retinal plasticity. (c) Development of retinal prosthesis for restoration of sight in patients who lost their photoreceptors due to retinal injury or disease. (**D**) The fourth thematic area was advanced microscopy and is aimed at development of microscope designs that can reveal molecular changes at the cellular scale in living tissues.

**A.1. HEARING:** Observing tissue damage and the healing response with cellular resolution and molecular specificity is essential for the effective development of innovative molecular therapies. For this purpose we have been developing miniature microscopes for use in the living body. We have developed a clinically deployable second-harmonic generation microendoscope that reveals specific patterns of tissue and cellular micro-architecture, and visualized sarcomere lengths and twitch contraction dynamics, and abnormalities in individual striated muscle fibers of humans. This tool was further modified for neurotology to visualize the inner ear and guide placement of cochlear implants after blast injury.

**A.2. WOUND HEALING.** We have used several *in vivo* and *in vitro* models of wound healing to study the basic cell and molecular mechanisms of repair. These are informative and continue to be used to reveal basic processes of wound healing. In the advancement of therapies for accelerating and improving wound healing, there is a need for predictive models of human wounds and response to intervention. We have been working on a number of rodent models of wound healing including an excision wound model. Since many of the battlefield wounds are accompanied by burn injury we have established burn models and evaluated therapies in these models. We have also evaluated these therapies in third degree burns on rats.

**A.3. VISION:** With increased prevalence of injury from the improvised explosive devices (IED) the potential for eye damage has increased. We study the mechanisms of corneal opacification following corneal injury, and develop strategies for preventing scarring and restoring corneal transparency. We also study the mechanisms of retinal injury and develop strategies for reduction of retinal scotomata (blind spots) and scarring based on our recently discovery of the adult retinal plasticity. In addition, we develop optoelectronic retinal prosthesis for restoring sight to patients who lost their photoreceptors due to mechanical or thermal injury.

**A.4. ADVANCED MICROSCOPY**. To reveal cellular and molecular changes associated with tissue damage and response to therapy we build implantable microscopes, which greatly enhances our capabilities in regenerative medicine. The microscope is based on a dual axis configuration that enables miniaturization and will be used to assess tissue regeneration and tissue response to novel therapies.

## B. STATEMENTS OF SIGNIFICANCE

**B.1. HEARING:** Hearing loss is a key health problem afflicting military personnel and the general public. Our work will lead to improved therapeutic approaches and novel prosthetic technologies for treating hearing loss due to inner ear damage or pathology. The clinical information we will obtain has the potential to fundamentally alter the diagnosis and treatment of human cochlear pathology. Our microscope designs will allow *in vivo* cellular level imaging of rapid biological dynamics at much faster speeds than currently possible, and enable the study of molecular processes using multiple probes and reagents.

**B.2. WOUND HEALING.** We have investigated strategies to selectively activate the lipid-encapsulated biomolecules using short pulses of near-infrared laser light for directed delivery of biomolecules and controlled tissue healing. To assess efficacy we have built have built multispectral, miniaturized confocal

microscopes that can be used at sites of injury and used to assess therapeutic outcome. The self-aligning system is simple and robust and will refine these studies and accelerate the analyses.

**B.3. VISION:** With increased prevalence of injury from the improvised explosive devices the potential for eye damage has increased. Thermal burns and mechanical damage to the cornea often result in its opacification leading to serious visual impairment. We study the mechanisms of tissue damage and develop precise surgical technologies for transparent ocular tissues. Shear forces inflicted by explosions or impact may result in traumatic retinopathy due to damage to retinal pigment epithelium and photoreceptors, leading to loss of sight. To restore vision in patients who lost their photoreceptors we were developing two strategies: (a) selective retinal therapy for reduction of localized scars and scotomata based on retinal plasticity, and (b) for patients with loss of photoreceptors in large areas we develop an opto-electronic retinal prosthesis that delivers visual information to the inner retinal neurons using electrical stimulation.

**B.4. ADVANCED MICROSCOPY**. Cellular level resolution of processes in hearing, vision and wound healing are essential to understanding mechanism and guiding interventions. New devices are developed and utilized in each of these three application areas.

## C. ACCOMPLISHMENTS

### HEARING

Throughout the history of surgery, new imaging technology has repeatedly led to new surgical techniques for accessing previously unreachable anatomic areas. This occurs because the ability to expose and examine tissues is essential to their successful manipulation. As examples, the binocular surgical microscope led to major advances in middle ear and neurosurgery. The laparoscope has irreversibly altered general surgery, and the arthroscope has changed orthopedics. The inner ear is one of the last areas of the body to remain largely inaccessible to direct examination and intervention. Our work in this area has aimed to remove this barrier.

Hearing loss related to inner ear disorders is a widespread problem that impacts about 28 million Americans and is an important issue for military veterans, many of whom have suffered hearing loss in the course of duty. Yet, otologists have been severely limited in their ability to diagnose even common pathology, let alone to treat disease in a non-destructive manner. For patients with sudden hearing loss, otologists are commonly list numerous potential causes before admitting the cause is unknown. Treatment is thus compromised, since the various potential causes may respond quite differently to specific interventions. Progress in treating hearing loss depends in large part on the invention of new minimally invasive technologies for visualizing the inner ear. We have created clinical instrumentation using micro-optics for this purpose.

This project was a collaboration between a biophysicist, Mark Schnitzer, whose lab invented novel minimally invasive imaging techniques known as fluorescence microendoscopy (FME), a physician scientist, Nikolas Blevins, who is a recognized expert in inner ear surgery and research, and an audiologist, Gerald Popelka, who is a co-inventor of the digital hearing aid. We have achieved exciting results imaging the inner ears of live guinea pigs, and have shown that FME can resolve cochlear structures in live subjects in a manner far superior to that of any other existing technology, with minimal impact on cochlear function. We achieved an important landmark in auditory science in being able to image the mammalian auditory hair cells that transduce acoustic pressure waves into the electrical signals that our brains perceive as sound. ***These mammalian hair cells have never been seen before in live subjects.***

Cochlear implantation represents a revolutionary medical technology. To date, approximately 100,000 prosthetic devices have been implanted in children and adults worldwide, allowing recipients to participate in the hearing world. Nonetheless, there is tremendous variability in patient outcomes, which remains largely unexplained. It is widely speculated that much of the variability may arise from differences in the number or spatial distribution of viable cochlear nerve fibers that remain available in the diseased ear to relay signals from an implant to the patient's brain.

The FME device was designed to be used intra-operatively immediately prior to implantation for non-destructive mapping of the neurons that project into these fibers. Maps of the location, density, and electrical sensitivity of these neurons and the proximal portions of the nerve fibers can be created based not only on anatomic appearance but also on neuronal activity as assessed optically. By correlating this information with each patient's post-implantation hearing performance we can: 1) design more effective implants; 2) perform superior surgical procedures in which implant electrodes are situated optimally to stimulate the neurons that remain active; and 3) customize the electrical characteristics of an implant to better suit a particular individual's inner ear structure and function. These advances were designed to expand the now stringent candidacy criteria for implantation, thereby allowing hearing restoration to far more patients. We created the instrumentation with potential for just this purpose.

Inspection of living hair cells required innovation of multiple elements: optical instrumentation, minimally invasive surgical methods, and creation of a custom-engineered ferromagnetic apparatus for flexibly positioning a microendoscope within the cranium. We used guinea pigs, a common model for otologic research due to the comparative similarity of the guinea pig cochlea to the human inner ear. Via hearing measures, histological analyses, and stereological counts of hair cells, we assessed and minimized microendoscopy's impact on cochlear function.

We created a suite of complementary surgical and optical techniques for visualizing the mammalian cochlea while retaining hearing capacity. Our approach uses minimally invasive insertion into the scala tympani of a 'needle-like' 500-μm- or 1000-μm-diameter microendoscope. These probes are composed of gradient refractive index micro-lenses, provide micron-scale resolution, and enable high-speed epi-fluorescence and three-dimensional, laser-scanning two-photon fluorescence imaging (**Fig. 1**).

Using novel, minimally invasive surgical methods and two-photon microendoscopy, we inspected the cochlea's hair cells, hair bundles, neurites, and actin micro-architecture in live guinea pigs. Measurements of hearing thresholds showed this combination induced a change in auditory sensitivity of only ~10-30 dB and thus preserved substantial hearing capability. This retention of auditory function was consistent with *post hoc* histological findings that microendoscopy had minimal impact on hair cells. Overall, the unprecedented capability to image a functional cochlea's basic elements for auditory transduction enables a wide range of future studies regarding the cellular characteristics of the inner ear and how cochlear cells respond to treatments for hearing loss. We have been working to bring this imaging apparatus into the otologic surgical setting.

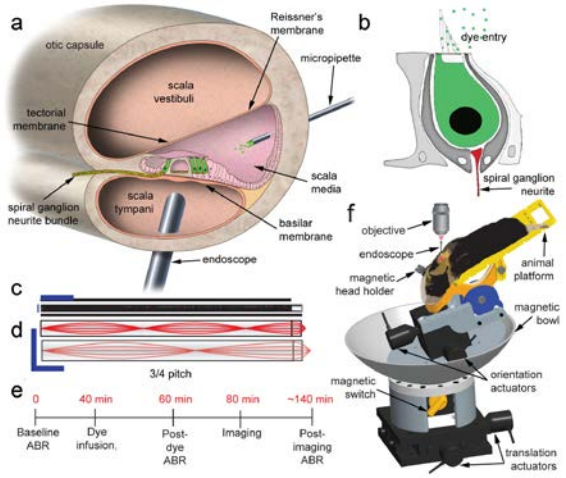


**Figure 1: Procedures for imaging auditory hair cells in live guinea pigs. (a)** A micropipette infused fluorescent dye into the scala media, the fluid bathing the hair cells (labeled green), via a pinhole cochleostomy that was later sealed. The microendoscope entered via a cochleostomy in the scala tympani and was situated beneath, but did not contact, the basilar membrane during imaging. **(b)** Upon infusion into the scala media, styryl dyes FM1-43 and AM1-43 quickly enter cochlear hair cells via auditory transduction channels in the stereocilia. These dyes label hair cells' cytoplasm (green) but neither the nuclei nor supporting cells that lack transduction channels. Intravital dye RH4-14 labels spiral ganglion neurites' membranes (red) *in vivo*. **(c)** Photograph of a compound doublet gradient refractive index (GRIN) lens microendoscope. The relay lens is coated black. The micro-objective is the uncoated lens at the rightward tip of the probe. Scale bar is 2 mm. **(d)** Optical ray trajectories for the microendoscope of panel c. The relay lens is 5/4 pitch in length, *i.e.* each ray's transverse coordinate undergoes 5/4 of a sinusoidal oscillation as the ray propagates along the optical axis. The micro-objective has a greater numerical aperture (0.43) than the relay (0.2) and is less than ¼ pitch in length. Horizontal and vertical scale bars are 2 mm and 1 mm, respectively. **(e)** Typical experimental timeline, with hearing sensitivity assessed via auditory brainstem response (ABR) measurements before, during, and after imaging. **(f)** A custom-engineered magnetic apparatus stabilizes the guinea pig's head and body. A magnet is cemented to the cranium and then locked into place with a rigid magnetic arm. Coarse and fine translation and orientation actuators allow precise positioning of the animal beneath the microendoscope, with the cochlea as center of rotation. A ~0.8–1.3 mm diameter cochleostomy with a post-auricular approach permits the microendoscope to enter the left cochlea's basal turn.

**Peer-reviewed publications from this project:**


1 Barretto, R. P., Ko, T. H., Jung, J. C., Wang, T. J., Capps, G., Waters, A. C., Ziv, Y., Attardo, A., Recht, L. & Schnitzer, M. J. Time-lapse imaging of disease progression in deep brain areas using fluorescence microendoscopy. *Nature Medicine* **17**, 223-228, doi:10.1038/nm.2292 (2011).

2 Barretto, R. P., Messerschmidt, B. & Schnitzer, M. J. In vivo fluorescence imaging with high-resolution microlenses. *Nature methods* **6**, 511-512, doi:10.1038/nmeth.1339 (2009).

3 Barretto, R. P. & Schnitzer, M. J. In vivo microendoscopy of the hippocampus. *Cold Spring Harbor Protocols* **2012**, 1092-1099, doi:10.1101/pdb.prot071472 (2012).

4 Barretto, R. P. & Schnitzer, M. J. In vivo optical microendoscopy for imaging cells lying deep within live tissue. *Cold Spring Harbor Protocols* **2012**, 1029-1034, doi:10.1101/pdb.top071464 (2012).

5 Cromie, M. J., Sanchez, G. N., Schnitzer, M. J. & Delp, S. L. Sarcomere lengths in human extensor carpi radialis brevis measured by microendoscopy. *Muscle & Nerve* **48**, 286-292, doi:10.1002/mus.23760 (2013).

6 Fitzgerald, J. E., Lu, J. & Schnitzer, M. J. Estimation theoretic measure of resolution for stochastic localization microscopy. *Physical review letters* **109**, 048102 (2012).
7 Ghosh, K. K., Burns, L. D., Cocker, E. D., Nimmerjahn, A., Ziv, Y., Gamal, A. E. & Schnitzer, M. J. Miniaturized integration of a fluorescence microscope. *Nature Methods* **8**, 871-878, doi:10.1038/nmeth.1694 (2011).
8 Marshall, J. D. & Schnitzer, M. J. Optical strategies for sensing neuronal voltage using quantum dots and other semiconductor nanocrystals. *ACS nano* **7**, 4601-4609, doi:10.1021/nn401410k (2013).
9 Mukamel, E. A. & Schnitzer, M. J. Unified resolution bounds for conventional and stochastic localization fluorescence microscopy. *Physical Review Letters* **109**, 168102 (2012).
10 Nimmerjahn, A., Mukamel, E. A. & Schnitzer, M. J. Motor behavior activates Bergmann glial networks. *Neuron* **62**, 400-412, doi:10.1016/j.neuron.2009.03.019 (2009).
11 Piyawattanametha, W., Cocker, E. D., Burns, L. D., Barretto, R. P., Jung, J. C., Ra, H., Solgaard, O. & Schnitzer, M. J. In vivo brain imaging using a portable 2.9 g two-photon microscope based on a microelectromechanical systems scanning mirror. *Optics Letters* **34**, 2309-2311 (2009).
12 Prakash, R., Yizhar, O., Grewe, B., Ramakrishnan, C., Wang, N., Goshen, I., Packer, A. M., Peterka, D. S., Yuste, R., Schnitzer, M. J. & Deisseroth, K. Two-photon optogenetic toolbox for fast inhibition, excitation and bistable modulation. *Nature Methods* **9**, 1171-1179, doi:10.1038/nmeth.2215 (2012).
13 St-Pierre, F., Marshall, J. D., Yang, Y., Gong, Y., Schnitzer, M. J. & Lin, M. Z. High-fidelity optical reporting of neuronal electrical activity with an ultrafast fluorescent voltage sensor. *Nature neuroscience* **17**, 884-889, doi:10.1038/nn.3709 (2014).
14 Wilt, B. A., Burns, L. D., Wei Ho, E. T., Ghosh, K. K., Mukamel, E. A. & Schnitzer, M. J. Advances in light microscopy for neuroscience. *Annual Review of Neuroscience* **32**, 435-506, doi:10.1146/annurev.neuro.051508.135540 (2009).

**VISION**

**Ablation and excision of transparent ocular tissues.** During the current funding period we studied the mechanisms of laser ablation and dissection of transparent ocular tissues for precise excision of the damaged corneal tissue. We demonstrated three distinct mechanisms of transparent tissue cutting with ultrashort pulse and UV lasers: thermal photoablation, photodissociation and plasma-mediated ablation. With ArF excimer laser (193nm) we have shown a single-photon photodissociation of the proteins. However, this process by itself cannot explain photoablation, which requires certain threshold radiant exposure for tissue ejection driven by overheating and explosive vaporization. With femtosecond laser we have observed multiphoton photodissociation below the threshold of plasma formation – a process which was not reported previously. The threshold of photodissociation was below the threshold of dielectric breakdown only for the wavelengths shorter than 532 nm. This process was overlooked so far since most of the fs lasers in ophthalmology operate at near-IR wavelengths. Multiphoton photodissociation may allow for excision of tissue without mechanical damage typically associated with the bubble formation following plasma-mediated breakdown, as illustrated in **Figure 2**. In addition, this process may allow altering refractive index of the transparent tissue – a novel method of non-invasive refractive correction.

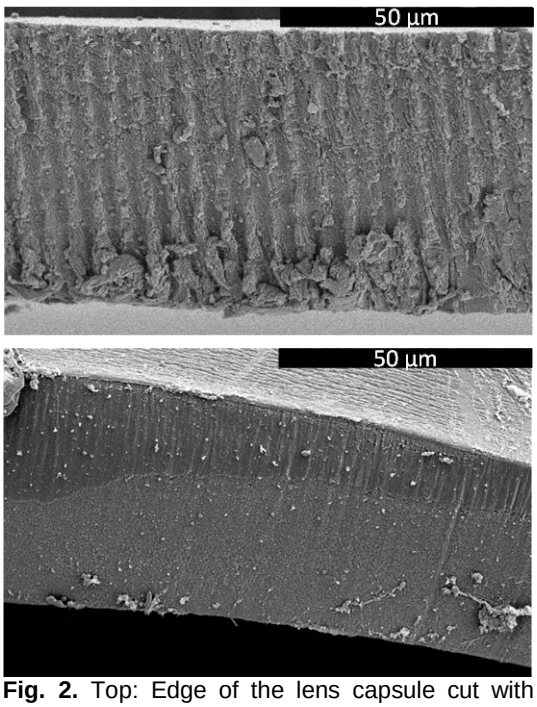


**Fig. 2.** Top: Edge of the lens capsule cut with 1030nm, 400fs laser at 10 uJ/pulse.
Bottom: same tissue cut with 400nm, 100fs laser at 0.02 uJ/pulse.

**Model of Traumatic Retinal Injury:**

We established an animal model of traumatic retinal injury involving mechanical breakage of the retina, Bruch's membrane and choroidal bleeding. This model involves a rapid scanning of the high power laser focused on the retina. With a scanning velocity of about 10 m/s and beam diameter about 100 um the

beam dwell time (exposure time of the tissue) is about 10 us. During such short time the heat is confined to cellular scale, therefore pigmented cells in the RPE and choroid can be selectively overheated and form cavitation bubbles around melanosomes. These bubbles mechanically rupture the cells, and if large enough, they can rupture Bruch's membrane and choroidal vasculature, causing bleeding. Since the mechanism of tissue damage is primarily mechanical, with minimal thermal effects, the damage closely resembles the typical results of the mechanical trauma.

**Migration of Photoreceptors for Elimination of Retinal Scars:**

We explored a possibility of eliminating scotomata and glial scars in the areas with traumatic loss of photoreceptors by inducing migration of the photoreceptors into the retinal damage zone. For this purpose we thermally damage the scar tissue and observe its contraction over time. We placed lesions with various levels of severity and size and we are followed them up with in-vivo imaging (OCT, autofluorescence), histologically and with functional molecular phenotyping. We have demonstrated that photoreceptors in rabbits can migrate into the damage zone and rewire to the inner retinal neurons (**Fig. 3**). These observations have been also cofinremed in human patients undergoing retinal photocoagulation, using year-long follow-up with Optical Coherence Tomography.

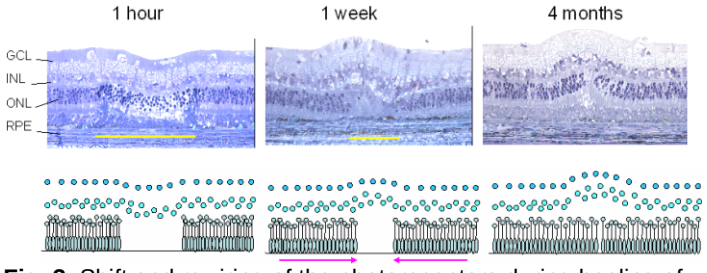


**Fig. 3.** Shift and rewiring of the photoreceptors during healing of the retinal lesion restores retinal continuity.

**Photovoltaic Retinal Prosthesis for Restoring Sight to the Blind:**

For the cases with massive loss of photoreceptors in large areas we developed a photovoltaic retinal prosthetic system, in which video information from a camera is displayed on video goggles, and imaged onto the subretinal implant using pulsed near-IR light. Each pixel in the subretinal photodiode array converts pulsed light into local electric current stimulating the residual retinal neurons. We fabricated photovoltaic arrays with pixels, each having 3 diodes connected in series between the central active and a circumferential return electrodes (**Fig. 4**). Pixel sizes of 280, 140 and 70 μm were compared. Experiments were conducted with wild type (WT, Long-Evans) and degenerate (RCS) rats in-vitro and in-vivo. Spikes in the retinal ganglion cells were reproducibly elicited in healthy and degenerate retinas by NIR stimulation with pulse durations in the range 0.5 – 10 ms using all 3 pixel sizes. The full-field stimulation thresholds with 4 ms pulses were 0.3 mW/mm$^2$ in WT retina and 0.8 mW/mm$^2$ in RCS retina. OCT and fluorescein angiography demonstrated normal retinal thickness and healthy vasculature above the implants upon 6 months follow-up. Visual Evoked Potential recordings in-vivo demonstrated stimulation thresholds in WT and RCS rats, similar to in-vitro levels: 0.5 mW/mm$^2$ with 4 ms pulses in WT and 1 mW/mm$^2$ in RCS rats - 2 orders of magnitude below the ocular safety limits. Due to optical activation of the pixels, the system is scalable to thousands of electrodes; it maintains the natural link between eye movements and image perception; the surgery is greatly simplified and modular design of the implant allows expanding the visual field by tiling. Such a versatile system could be used to address the divergent needs of patients with various forms of photoreceptor loss.

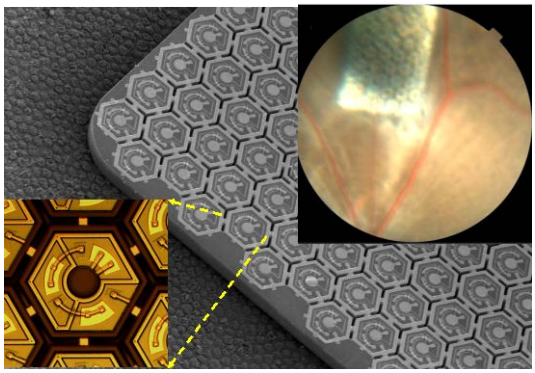

**Fig. 4.** Photovoltaic array under the retina in a rat eye. Left: Higher magnification view of a single pixel in the implant.

We have demonstrated that spatial resolution of the retinal response to photovoltaic stimulation in-vitro is limited by the pixel spacing – 65 um. Similarly, using Visually Evoked Potentials recordings in rats in-vivo, we demonstrated that grating visual acuity corresponds to the spacing of adjacent rows in the implant – 65 um. This is only twice below the normal acuity in rats – 30 um. If these results translate to human retina, it will correspond to visual acuity of about 20/250. With eye scanning and perceptual learning it might even cross the threshold of legal blindness in US – 20/200.

**Peer-reviewed publications in from this project:**


1. Inner Retinal Preservation in Rat Models of Retinal Degeneration Implanted with Subretinal Photovoltaic Arrays. J.G. Light, J.W. Fransen, A.N. Adekunle, A. Adkins, G. Pangeni, J. Loudin, K. Mathieson, D.V. Palanker, M.A. McCall, M.T. Pardue. *Exp. Eye Research* **128**: 34-42 (2014).
2. Performance of Photovoltaic Arrays in-vivo and Characteristics of Prosthetic Vision in Animals with Retinal Degeneration. H. Lorach, G. Goetz, Y. Mandel, X. Lei, T. Kamins, K. Mathieson, P. Huie, R. Dalal, J.S. Harris, D. Palanker. *Vision Research* 2014 [Epub ahead of print].
3. Selectivity of Direct and Network-mediated Stimulation of the Retinal Ganglion Cells with Epi-, Sub- and Intra-Retinal Electrodes. D. Boinagrov, S. Pangratz-Fuehrer, G. Goetz, D. Palanker. *Journal of Neural Engineering*, **11**: 026008 (11pp) (2014).
4. Cortical Responses Elicited by Photovoltaic Subretinal Prostheses Exhibit Similarities to Visually Evoked Potentials. Y. Mandel, G. Goetz, D. Lavinsky, P. Huie, K. Mathieson, L. Wang, T. Kamins, L. Galambos, R. Manivanh, J. Harris, D. Palanker. *Nature Communications **4**: 1980-* (2013).
5. Restoration of Retinal Structure and Function after Selective Photocoagulation. A. Sher, B.W. Jones, P. Huie, Y.M. Paulus, D. Lavinsky, L.S. Leung, H. Nomoto, C. Beier, R.E. Marc, and D. Palanker. *The Journal of Neuroscience* **33(16)**: 6800 – 6808 (2013).
6. Restoration of retinal morphology and residual scarring after photocoagulation. Lavinsky D, Cardillo JA, Mandel Y, Huie P, Melo LA, Farah ME, Belfort R, Palanker D. *Acta Ophthalmol*. 91(4): e315–e323 (2013).
7. Upper Threshold of Extracellular Neural Stimulation. D. Boinagrov, S. Pangratz-Fuehrer, B. Suh, K. Mathieson, N. Naik, D. Palanker. *Journal of Neurophysiology*, **108**: 3233-3238 (2012).
8. Photovoltaic retinal prosthesis: implant fabrication and performance. L Wang, K Mathieson, T I Kamins, J D Loudin, L Galambos, G Goetz, A Sher, Y Mandel, P Huie, D Lavinsky, J S Harris and D V Palanker. *Journal of Neural Engineering* **9**: 046014 (11pp) (2012)
9. Photovoltaic Retinal Prosthesis with High Pixel Density. K. Mathieson, J. Loudin, G. Goetz, P. Huie, L. Wang, T.I. Kamins, L. Galambos, R. Smith, J.S. Harris, A. Sher, D. Palanker. *Nature Photonics*, **6(6)**: 391–397 (2012).
10. Photodiode Circuits for Retinal Prostheses. J.D. Loudin, S.F. Cogan, K. Mathieson, A. Sher, and D.V. Palanker. IEEE TRANSACTIONS ON BIOMEDICAL CIRCUITS AND SYSTEMS, 1932-4545 (2011)
11. Non-damaging Retinal Phototherapy: Dynamic Range of Heat Shock Protein Expression. C. Sramek, M. Mackanos, R. Spitler, L.S. Leung, H. Nomoto, C. Contag, D. Palanker. *Invest. Ophthalmol. Vis. Sci.* **52(3)**:1780-7 (2011).
12. Multi-Focal Laser Surgery: Cutting Enhancement by Hydrodynamic Interactions Between Cavitation Bubbles. I. Toytman, A. Silbergleit, D. Simanovski, D. Palanker. *Physical Review E* (2010)
13. Optical breakdown in transparent media with adjustable axial length and location. I. Toytman; D. Simanovski; D. Palanker. *Optics Express*. **18(24)**: 24688-24698 (2010).


**ADVANCED MICROSCOPY**

Out of frustration with the archaic manner with which diagnoses are made in clinical medicine and are striving to bring this field into the 21st century. Currently, histopathological diagnosis is made using dyes and microscopes that are not too different from what we used 100 years ago. Given the optical tools available today we should be able to both refine and accelerate the diagnostic process. Toward this objective, we are advancing the field of point-of-care pathology and bringing the patient and the diagnostic event closer in both time and space. At present, diagnosis is made on biopsy samples that are examined, cut, sent to pathology laboratories, fixed, embedded in paraffin, sectioned, stained, and then examined under a microscope. The aim of these studies was to miniaturize the microscope (**Fig. 5**) such that if can be put it on, or in, the patient and

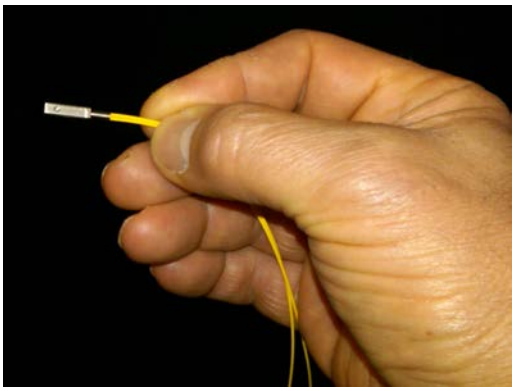

**Fig. 5.** Miniature Dual Axis confocal microscope.

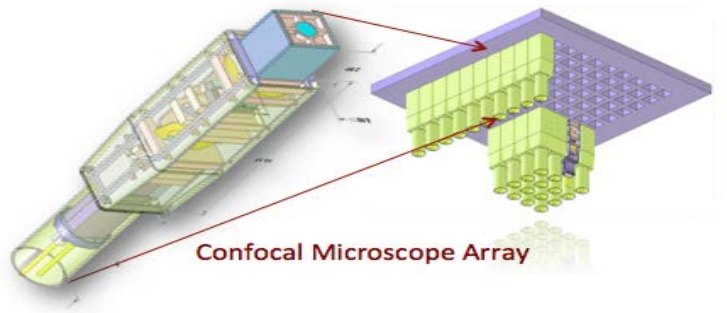


**Fig. 6.** Arrays of microscopes to increase throughput.

make the diagnosis at the point of care. Our miniature microscopes can image into tissue and look for multiple markers of wound healing. This miniature device can be cheaply and easily mass-produced, so we are developing arrays of microscopes (**Fig. 6**) to accelerate the process. The scanning of the tissue can be automated and the interpretation of the data computerized to guide and inform the clinician. This will enable examination of more tissue with greater anatomic and molecular accuracy than could be done by a pathologist sitting at a microscope. To improve the initial exam of the tissue and to guide the microscope(s) placement, we have developed a wide-field scanner (**Fig. 7**) that can be used in combination with the microscope array to quickly scan any excised tissue looking for the hallmarks of tissue damage. The tissue scanner and the microscope arrays used together provide both a macroscopic and a microscope view of the tissue. The two tools are complementary and designed to change how we make diagnosis.

**Fig. 7.** High-resolution tissue scanner to accelerate and refine pathological assessment.

The laser output in the DAC microscopes is coupled into a single-mode fiber with a GRIN collimator. The collimated beam is focused by a parabolic mirror, reflects off the microelectromechanical system (MEMS) scanner, and continues through the hemispherical lens. The focus of the illumination beam is imaged through the other optical branch, and the collected signal is amplified by a photomultiplier tube (PMT). As the MEMS mirror scans the focused spot across the sample, each pixel is displayed on the computer screen as an en-face image. We have published extensively on this basic design emphasizing the simplicity that allows for miniaturization, the increased dynamic range of a dual axis architecture relative to a single axis confocal scope, its multispectral and 3D scanning capabilities and the broad applicability in biomedical research. Since its inception as a breadboard prototype we have worked to scale the optical platform into progressively smaller devices as shown in **Figure 4**. In the first step of this process we developed the 10-mm-diameter “handheld” DAC system, which operates at 488 nm, 560 nm, 660 nm, 785 nm, and 1310 nm, and has been used extensively to image cells and tissues in mouse models of human biology and various human diseases**.** We are currently in the process of adapting this device to perform high speed one-dimensional scanning for the purpose of counting fluorescently labeled circulating cells as they course through individual blood vessels, and this application will be used in our experiments to detect and enumerate immune cells as an in vivo flow cytometer. The second step of miniaturization yielded the 5-mm-diameter DAC endomicroscope designed for imaging at 785 nm wavelength. Its small physical dimensions allow the endomicroscope to fit in the instrument channel of a therapeutic upper GI endoscope as shown in

The DAC microscope is a point scanning device, i.e., it images one voxel at a time. A key enabling component of the system is the mechanism that allows the voxel to be scanned to form an image. For miniaturized, implantable DACs, the scanners must be compact, mechanically robust, and able to provide 3-D scanning to form volumetric images. The principal design features of the 3.8 mm multispectral DAC are two spherical reflective surfaces facing each other, and two MEMS scanners facing away from each other in a configuration that allows the beams to scan into tissue from the side of the package. A first spherical mirror having an outside diameter (OD) of 3.5 mm is used to re-collimate the beams diverging from the focal point of a “mixing lens”, which creates a common point-of-focus of beams emerging from

two single-mode fibers. A second spherical mirror is then used to focus the beams into the tissue at a predetermined depth of 0-300 μm. The use of two symmetrically placed spherical mirrors thus provides the necessary collimation, alignment, and focusing of light along beam paths inside the endomicroscope, and inside the tissue. There are two important advantages gained by this optical design. First, by using reflective type focusing optics, we get improved achromatic operation that enables simultaneous fluorescence imaging at multiple wavelengths over the whole visible-NIR optical window of tissue from 488 nm to 830 nm. Second, the improved simplicity and symmetry of this design simplifies the assembly and reduces alignment tolerances during fabrication, thus allowing an economical solution for scaling down the endomicroscope dimensions. A first MEMS scanner is used for providing fast depth scanning of the beams within the tissue by using a high frequency piston-motion mirror that rapidly produces different imaging depths along the z-direction (axial scanner). In addition, a second MEMS scanner placed at 45 degrees with respect to the package axis in order to provide side-looking beams, uses a rapidly oscillating mirror that tips and tilts about the X and Y axes, respectively to produce high frequency lateral scanning of the beams, thereby producing an X-Y image plane at any one of the specific image depths determined by the axial scanner. Both types of scanners are combined in a 3-D MEMS scanner assembly to provide a high-speed “all-MEMS” 3-D scanning system.

The scanning of different imaging depths is produced by Z-shifting of the 1-Daxial scanner, while the transverse scanning of the image-point is achieved by the 2-D lateral scanner. By using the axial scanner to rapidly vary the imaging depth, the X-Y image plane produced by the 2-D scanner is effectively scanned deeper into the tissue, thereby enabling faster “all-MEMS” scanning in 3-D. The feature of real-time depth scanning gives the DAC endomicroscope the ability to produce axially-penetrating, “OCT-like”, fluorescence images, which are important for examining disease in living subjects at the cellular level using fluorescent molecular probes. Both scanners have two separate reflectors in the same scanning plane for simultaneous scanning of the illumination and collection beam, and are actuated by self-aligned vertical comb drives[1]. The 2-D lateral scanner consists of outer and inner torsional springs for rotation around two orthogonal axes. The 1-D axial scanner is held by four springs to produce stable up-and-down piston motion. The springs have serpentine design to minimize their stiffness in the up-down direction while minimizing the spring area.

**Peer-reviewed Publications from this Project:**


1. Liu, J. T., Loewke, N. O., Mandella, M. J., Leigh, S. Y., Levenson, R. M., Crawford, J. M. & Contag, C. H. Real-time pathology through in vivo microscopy. *Studies in Health Technology and Informatics* **185**, 235-264 (2013).
2. Leigh, S. Y. & Liu, J. T. Multi-color miniature dual-axis confocal microscope for point-of-care pathology. *Optics Letters* **37**, 2430-2432, doi:10.1364/OL.37.002430 (2012).
3. Lo, D. D., Mackanos, M. A., Chung, M. T., Hyun, J. S., Montoro, D. T., Grova, M., Liu, C., Wang, J., Palanker, D., Connolly, A. J., Longaker, M. T., Contag, C. H. & Wan, D. C. Femtosecond plasma mediated laser ablation has advantages over mechanical osteotomy of cranial bone. *Lasers in Surgery and Medicine* **44**, 805-814, doi:10.1002/lsm.22098 (2012).
4. Piyawattanametha, W., Ra, H., Qiu, Z., Friedland, S., Liu, J. T., Loewke, K., Kino, G. S., Solgaard, O., Wang, T. D., Mandella, M. J. & Contag, C. H. In vivo near-infrared dual-axis confocal microendoscopy in the human lower gastrointestinal tract. *Journal of Biomedical Optics* **17**, 021102, doi:10.1117/1.JBO.17.2.021102 (2012).
5. Loewke, K. E., Camarillo, D. B., Piyawattanametha, W., Mandella, M. J., Contag, C. H., Thrun, S. & Salisbury, J. K. In vivo micro-image mosaicing. *IEEE transactions on Bio-medical Engineering* **58**, 159-171, doi:10.1109/TBME.2010.2085082 (2011).
6. Ra, H., Piyawattanametha, W., Gonzalez-Gonzalez, E., Mandella, M. J., Kino, G. S., Solgaard, O., Leake, D., Kaspar, R. L., Oro, A. & Contag, C. H. In vivo imaging of human and mouse skin with a handheld dual-axis confocal fluorescence microscope. *The Journal of Investigative Dermatology* **131**, 1061-1066, doi:10.1038/jid.2010.401 (2011).
7. Liu, J. T., Loewke, N. O., Mandella, M. J., Levenson, R. M., Crawford, J. M. & Contag, C. H. Point-of-care pathology with miniature microscopes. *Analytical Cellular Pathology* **34**, 81-98, doi:10.3233/ACP-2011-011 (2011).

8. Mackanos, M. A., Helms, M., Kalish, F. & Contag, C. H. Image-guided genomic analysis of tissue response to laser-induced thermal stress. *Journal of Biomedical Optics* **16**, 058001, doi:10.1117/1.3573387 (2011).
9. Ra, H., Gonzalez-Gonzalez, E., Smith, B. R., Gambhir, S. S., Kino, G. S., Solgaard, O., Kaspar, R. L. & Contag, C. H. Assessing delivery and quantifying efficacy of small interfering ribonucleic acid therapeutics in the skin using a dual-axis confocal microscope. *Journal of Biomedical Optics* **15**, 036027, doi:10.1117/1.3432627 (2010).
10. Liu, J. T., Mandella, M. J., Loewke, N. O., Haeberle, H., Ra, H., Piyawattanametha, W., Solgaard, O., Kino, G. S. & Contag, C. H. Micromirror-scanned dual-axis confocal microscope utilizing a gradient-index relay lens for image guidance during brain surgery. *Journal of Biomedical Optics* **15**, 026029, doi:10.1117/1.3386055 (2010).
11. Gonzalez-Gonzalez, E., Ra, H., Spitler, R., Hickerson, R. P., Contag, C. H. & Kaspar, R. L. Increased interstitial pressure improves nucleic acid delivery to skin enabling a comparative analysis of constitutive promoters. *Gene Therapy* **17**, 1270-1278, doi:10.1038/gt.2010.74 (2010).
12. Liu, J. T., Mandella, M. J., Crawford, J. M., Contag, C. H., Wang, T. D. & Kino, G. S. Efficient rejection of scattered light enables deep optical sectioning in turbid media with low-numerical-aperture optics in a dual-axis confocal architecture. *Journal of Biomedical Optics* **13**, 034020, doi:10.1117/1.2939428 (2008).
13. Ra, H., Piyawattanametha, W., Mandella, M. J., Hsiung, P. L., Hardy, J., Wang, T. D., Contag, C. H., Kino, G. S. & Solgaard, O. Three-dimensional in vivo imaging by a handheld dual-axes confocal microscope. *Optics Express* **16**, 7224-7232 (2008).
14. Liu, J. T., Mandella, M. J., Ra, H., Wong, L. K., Solgaard, O., Kino, G. S., Piyawattanametha, W., Contag, C. H. & Wang, T. D. Miniature near-infrared dual-axes confocal microscope utilizing a two-dimensional microelectromechanical systems scanner. *Optics Letters* **32**, 256-258 (2007).
15. Liu, J. T., Mandella, M. J., Friedland, S., Soetikno, R., Crawford, J. M., Contag, C. H., Kino, G. S. & Wang, T. D. Dual-axes confocal reflectance microscope for distinguishing colonic neoplasia. *Journal of Biomedical Optics* **11**, 054019, doi:10.1117/1.2363363 (2006).